

Research Article

Roland Tolulope Loto*

Effect of chloride concentration on the corrosion resistance of pure Zn metal in a 0.0626 M H₂SO₄ solution

<https://doi.org/10.1515/eng-2022-0445>

received March 11, 2023; accepted April 23, 2023

Abstract: The aftermath of Cl⁻ anion concentration reactions on the corrosion resistance of pure Zn metal in 0.0625 M H₂SO₄ was examined by potentiodynamic polarization, optical representations, scanning electron image analysis, energy dispersive X-ray (EDX) spectroscopy, open-circuit potential analysis, X-ray diffractometry, weight loss method and X-ray fluorescence. The results show that the degradation of Zn increased with an increase in the chloride concentration from 4.089 and 0.218 mm/year to 10.085 and 4.015 mm/year (polarization and weight loss). The corrosion potential at 0.0625 M H₂SO₄ to 0.0625 M H₂SO₄/0.5% NaCl concentration displayed minimal variation (-1.535 to -1.519 V), whereas a significant shift was observed for the plots at 0.0625 M H₂SO₄/1% NaCl and 0.0625 M H₂SO₄/2% NaCl (-1.384 and -0.932 V). The weight loss plot at all Cl⁻ anion concentrations displayed an ordered decrease in the corrosion rate analogous to exposure times. The scanning electron microscopic images of Zn in 0.0625 M H₂SO₄/2% NaCl solution showed significant deterioration and corrosion pits. The image at 0.0625 M H₂SO₄ solution revealed limited localized and general surface deterioration, while the corresponding EDX data depict the presence of S. The Zn open-circuit potential plot from a 0.0625 M H₂SO₄ solution was relatively electropositive compared to the plot from a 0.0625 M H₂SO₄/2% NaCl solution. Both plots exhibited limited reactive-inert transition properties and attained relative thermodynamic equilibrium after 600 s of exposure with final corrosion potentials of -0.91 and -0.97 V at 7,200 s. Zn was the only crystallographic phase identified on its surface before corrosion, whereas ZnS, ZnFeS, ZnMnS, ZnMnFeS, and ZnMg₄ corrosion products were identified after corrosion.

Keywords: zinc, corrosion management, NaCl, environmental degradation, H₂SO₄

1 Introduction

Ferrous alloys such as stainless steels, carbon steels, tool steels, low-grade alloys, etc., are the most applicable materials currently in use worldwide coupled with ongoing research to improve their engineering properties for optimal application in astringent environments [1–6]. However, they are prone to corrosion leading to economic and financial loss in a variety of industries [7–9]. Protection of steel parts, structures, columns, fittings, pipes and components is of utmost economic importance [10,11]. One of the most cost-effective, versatile, resilient and proven methods for the protection of steel is by Zn coatings. Zn offers significant cost-effective protection against metallic corrosion in atmospheric environments through cold-dip galvanizing, hot-dip galvanizing, galvannealing, electro-galvanizing, continuous-line galvanizing, zinc plating and spraying, mechanical plating and zinc-pigment paints [12]. Zn is the fourth most utilized metal globally with about 50% of Zn production applied in Zn galvanizing processes [13]. It represents the 23rd most available material in the earth's encrustation at 0.013%. The most common application of Zn is its usage as an anti-corrosion coating [14,15]. Other applications include white pigmentation in paints, catalyst in rubber production, manufacture of protective agents for rubber polymers and plastics, production of photocopying materials [16,17], propellant in model rockets [18], and corrosion protection for roofing sheets and petrochemical infrastructure [19,20]. The exceptional corrosion resistance of Zn is due to the evolution of a barrier coating that stifles further corrosion of the Zn surface by its exposure to atmospheric elements such as fog, rain, gases, dew, soot, snow, humidity and reactive dust. The reaction of Zn with O₂ results in the formation of a thin, corrosion-resistant oxide layer that further reacts with moisture leading to the formation of zinc hydroxide

* Corresponding author: Roland Tolulope Loto, Department of Mechanical Engineering, Covenant University, Ota, Ogun State, Nigeria, e-mail: tolu.loto@gmail.com

and, subsequently, resilient and chemically stable zinc carbonate after reacting with CO_2 [21]. Zn corrosion is influenced by the environment in which it is applied [22,23]. Salt composition within marine conditions significantly influences Zn corrosion [24]. Nevertheless, coatings of Zn have been applied for generations to protect steel from corrosion with some coatings still very effective after a century. Zn and metallic parts coated with Zn exhibits substantially extended operational lifespan compared to some other alloys exposed to the atmosphere.

2 Experimental methods

2.1 Materials and preparation

Square-shaped Zn sheets with surface proportions of 100 mm × 100 mm × 50 mm (length, breadth and thickness) were split into seven work samples with dimensions of 1 cm × 2 cm using a manual hand tool for weight loss measurement, potentiostatic analysis and open-circuit potential evaluation. Elemental analysis of the Zn work piece was performed with a PhenomWorld high-resolution electron microscope at the Covenant University Central Instrumentation Research Facility, Ota, Ogun State, Nigeria. The energy dispersive X-ray (EDX) microanalysis, represented in Figure 1, shows the Zn spectrum image with wt% compositions of 100% metallic Zn. Cu cables were affixed to Zn workpieces with soft solder before being enmeshed pre-solidified acrylic paste. The exterior area of the Zn workpiece was graded with SiC sheets (60–1,500 grits), brightened with a 3 μm diamond mixture and washed with de-mineralized H_2O and dimethyl ketone. And 0.0625 M H_2SO_4 solution was concocted from standard class H_2SO_4 acid solution. The recrystallized

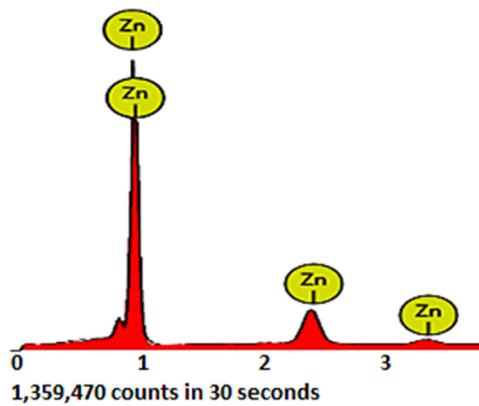


Figure 1: EDS spectrum for Zn workpieces.

NaCl at 0.0625, 0.125, 0.25, 0.5 and 1% was added to the acid solution. The electrochemical and weight measuring instruments were checked for any likelihood of systematic anomalies. The performance of both instruments is limited by their precision and accuracy. Instrument calibration, hardware test and test for reproducibility of consistent results were done for the instruments.

2.2 Potentiodynamic polarization and open-circuit potential evaluation

Corrosion kinetics was evaluated by potentiodynamic polarization while corrosion thermodynamics was determined by open-circuit potential evaluation. Both tests were done at 308 K (ambient temperature) by adopting a Digi-Ivy 2311 potentiostatic apparatus. The apparatus, which consists of a triple cord electrode (Zn workpiece electrode, Ag/AgCl threshold electrode and Pt cord counter electrode), was networked to a laptop computer. Polarization data lines were drawn at a plot progression of 0.0015 V/s initiating at -1.55 to $+1.1$ V. The corrosion potential, C_p (V), and the corrosion current density, C_j (A/cm^2), values were acquired by Tafel computation. The corrosion rate, C_r (mm/year), is quantified from the following numerical values:

$$C_{RT} = \frac{0.00327 \times C_j \times C_q}{D}, \quad (1)$$

where E_w is the equivalent weight (g) of Zn, 0.00327 is the corrosion constant, and D is the density (g/cm^3). The polarization resistance, P_{rt} (Ω), is determined from the numerical formula:

$$P_{rt} = 2.303 \frac{B_a B_c}{B_a + B_c} \left(\frac{1}{I_{cr}} \right), \quad (2)$$

where B_a and B_c are anodic and cathodic Tafel slopes (V/dec).

2.3 Weight loss measurement

The Zn workpieces were placed in 200 mL of a 0.0625 M H_2SO_4 solution at NaCl concentrations of 0.0625, 0.125, 0.25, 0.5, 1 and 2% for 168 h of exposure. The weight measurement of Zn was done once in 24 h. The corrosion rate, C_{RT} (mm/year), is calculated as:

$$C_{RT} = \left[\frac{87.6 W_L}{DA t} \right], \quad (3)$$

where W_L is the weight loss (g), D is the density (g/cm^3), t is the time (h), A is the exposed surface area of the Zn workpiece (cm^2) and 87.6 is a constant for the corrosion rate.

2.4 Scanning electron microscopy (SEM), EDX and optical microscopy analysis

The Zn workpieces were suspended for 240 h in the acid-chloride solution. SEM images of Zn were obtained using a PhenomWorld scanning electron microscope prior to and following the corrosion test. Optical illustrations of Zn workpieces prior to and following the weight loss test at specific NaCl concentrations in the acid media were obtained and studied with an Omax trinocular metallurgical microscope and USB digital microscope after weight loss evaluation.

2.5 X-ray diffractometry (XRD) and X-ray fluorescence (XRF)

XRD data and the information on the component phases, compounds, impurities, precipitates, etc., on Zn workpieces from weight loss tests at a specific NaCl concentration, were obtained after scanning with a Rigaku D/Max-III C X-ray diffractometer at a sweep rate of $2^\circ/\text{min}$ within $2-50^\circ$ at ambient temperature with a Cu K-alpha radiation established at 40 kV and 20 mA in 2θ . The diffraction results (correlation magnitude) received were compared to threshold results obtained from the mineral powder diffraction folder

(ICDD) containing the threshold information of over 3,000 minerals. The composition of the Zn surface and its corroded specimens was evaluated using a Lab-X3500 Benchtop XRF Analyser with detection limits at ppm to 100%. The Lab-X 3500 instruments are fitted with Oxford Instruments Analytical Software Package, ASP3500, and pre-defined calibrations.

3 Results and discussion

3.1 Potentiodynamic polarization and optical microscopy characterization

Potentiodynamic polarization plots produced from the Zn reaction in 0.0625 M H_2SO_4 , 0.0625 M $\text{H}_2\text{SO}_4/0.0625\%$ NaCl, 0.0625 M $\text{H}_2\text{SO}_4/0.125\%$ NaCl, 0.0625 M $\text{H}_2\text{SO}_4/0.25\%$ NaCl, 0.0625 M $\text{H}_2\text{SO}_4/0.5\%$ NaCl, 0.0625 M $\text{H}_2\text{SO}_4/1\%$ NaCl and 0.0625 M $\text{H}_2\text{SO}_4/2\%$ NaCl solutions are represented in Figure 2. Table 1 shows the potentiodynamic data retrieved from the plots. Figure 3a–d shows the optical images of the Zn surface after the polarization test. The plots at 0.0625 M H_2SO_4 to 0.0625 M $\text{H}_2\text{SO}_4/0.5\%$ NaCl concentrations displayed minimal variation in corrosion potentials, i.e., from -1.535 to -1.519 V compared to the plots at 0.0625 M $\text{H}_2\text{SO}_4/1\%$ NaCl and 0.0625 M $\text{H}_2\text{SO}_4/2\%$ NaCl solutions exhibiting corrosion potential values of -1.384 and -0.932 V. This variation is due to the effect of the Cl^- anion concentration within the electrolyte, which influenced the redox reaction behavior of Zn. Zn corrodes relatively slower at a low Cl^- anion concentration due to the evolution of a protective oxide on its surface [25]. The Cl^- anions within the acid electrolyte diffuse

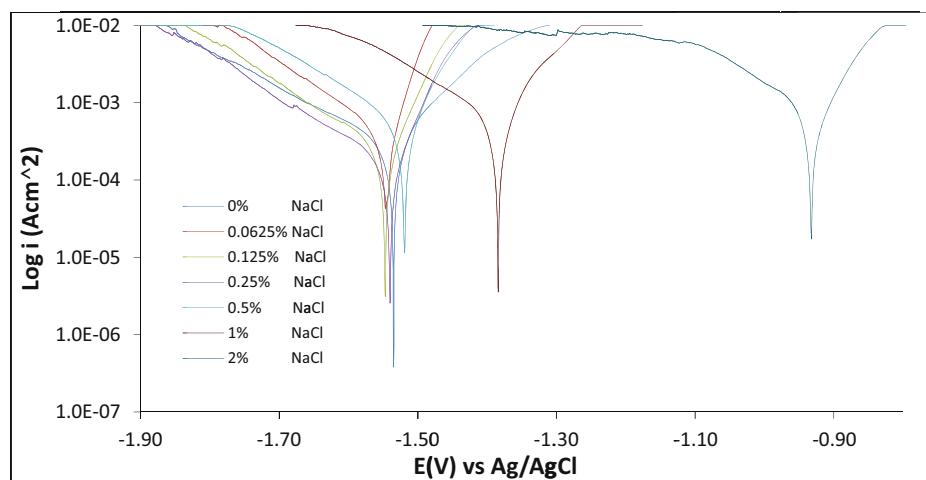


Figure 2: A potentiodynamic polarization plot of Zn in a 0.0625 M H_2SO_4 to 0.0625 M $\text{H}_2\text{SO}_4/2\%$ NaCl solution.

Table 1: Potentiodynamic polarization data for Zn corrosion in a 0.0625 M H₂SO₄/2% NaCl solution

| Sample | NaCl concentration (%) | Corrosion rate, C _R (mm/year) | Corrosion current, I (A) | Corrosion current density, J (A/cm ²) | Corrosion potential, C _p (V) | Polarization resistance, R _p (Ω) | Cathodic Tafel slope, B _c (V/dec) | Anodic Tafel slope, B _a (V/dec) |
|--------|------------------------|--|--------------------------|---|---|---|--|--|
| A | 0 | 4.089 | 3.48 × 10 ⁻⁴ | 2.74 × 10 ⁻⁴ | -1.535 | 73.76 | -4.399 | 8.414 |
| B | 0.0625 | 4.118 | 3.51 × 10 ⁻⁴ | 2.76 × 10 ⁻⁴ | -1.547 | 73.44 | -5.984 | 1.221 |
| C | 0.125 | 4.127 | 3.52 × 10 ⁻⁴ | 2.77 × 10 ⁻⁴ | -1.547 | 73.08 | -4.546 | 15.810 |
| D | 0.25 | 5.259 | 4.48 × 10 ⁻⁴ | 3.53 × 10 ⁻⁴ | -1.540 | 61.60 | -4.627 | 15.400 |
| E | 0.5 | 6.515 | 5.55 × 10 ⁻⁴ | 4.37 × 10 ⁻⁴ | -1.519 | 48.54 | -2.568 | 14.020 |
| F | 1 | 7.398 | 6.30 × 10 ⁻⁴ | 4.96 × 10 ⁻⁴ | -1.384 | 39.70 | -3.334 | 13.250 |
| G | 2 | 10.085 | 8.59 × 10 ⁻⁴ | 6.77 × 10 ⁻⁴ | -0.932 | 29.90 | -4.495 | 11.860 |

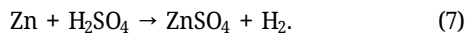
through the protective oxide film, causing corrosion of Zn [26,27]. Zn corrosion in acid chloride solutions occurs through two processes [28]. The cathodic half-cell is the reduction of O₂ and evolution of H₂ gas:



The corresponding anodic half-cell reaction is the oxidation of Zn:



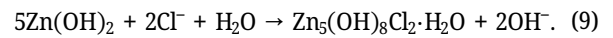
Zn²⁺ reacts with H⁺ ions and SO₄²⁻ ions according to the following equation:



The Zn²⁺ and 2OH⁻ ions react to produce Zn(OH)₂ [29]:



The Cl⁻ anions transport to anodic sites resulting in the formation of Zn₅(OH)₈Cl₂:



The polarization plots at 0.0625 M H₂SO₄ to 0.0625 M H₂SO₄/0.125% NaCl concentrations displayed a cathodic potential shift due to the collapse of the inert oxide [30,31], whereas from 0.0625 M H₂SO₄/0.25% NaCl to 0.0625 M H₂SO₄/2% NaCl concentrations, the corrosion potential shift was anodic. Beyond a 0.0625 M H₂SO₄/0.125% NaCl concentration, the reaction effect of Cl⁻ anions on the Zn surface in the H₂SO₄ solution surpassed the ZnO on the Zn surface leading to its deterioration.

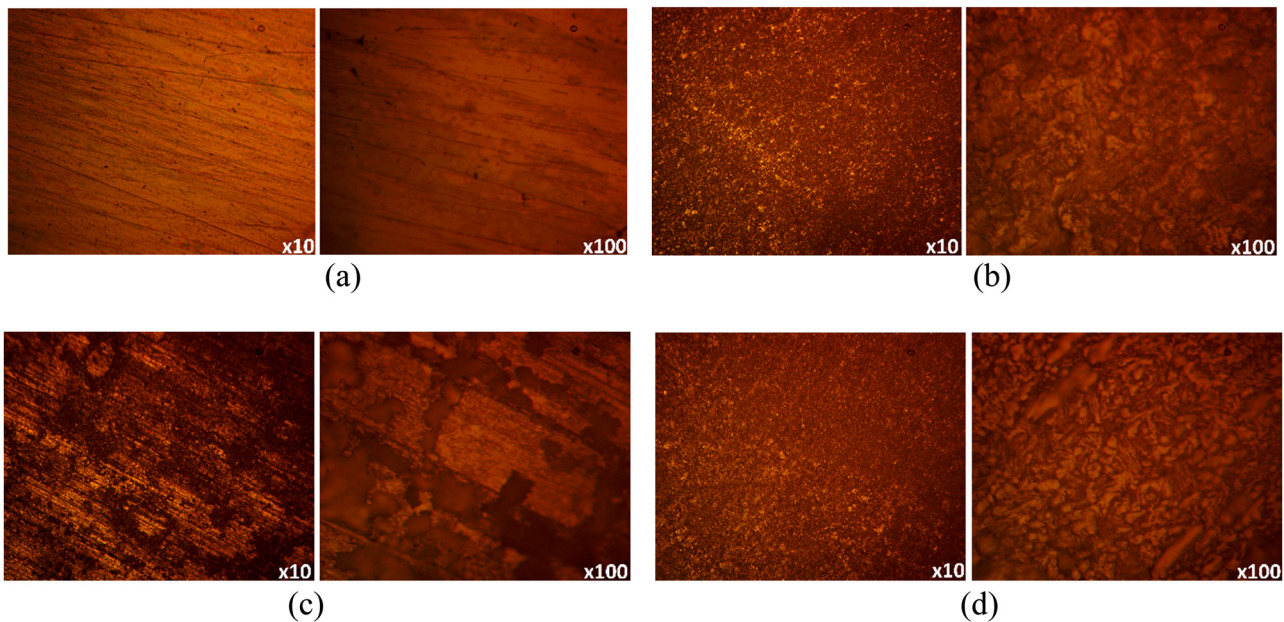


Figure 3: Optical representations of Zn surfaces: (a) preceding corrosion, (b) following corrosion in 0.0625 M H₂SO₄, (c) following corrosion in 0.0625 M H₂SO₄/0.0625% NaCl and (d) following corrosion in 0.0625 M H₂SO₄/2% NaCl.

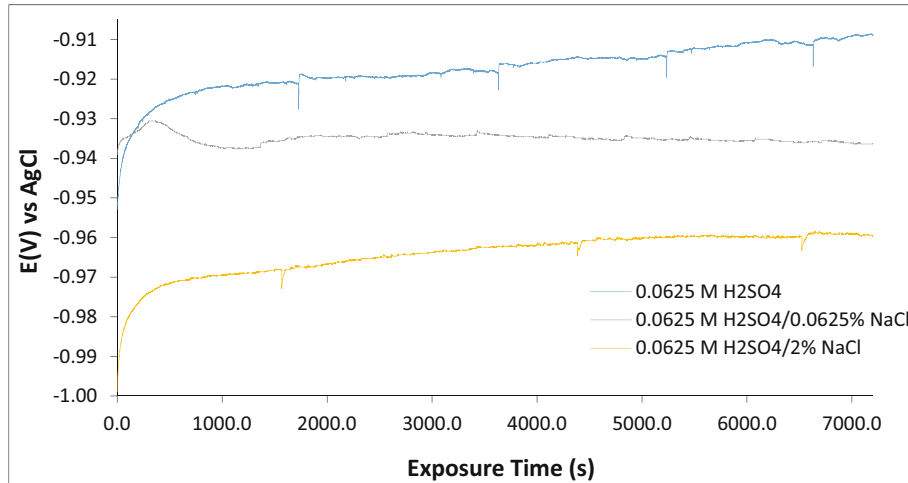


Figure 4: An open-circuit potential plot for Zn corrosion in 0.0625 M H_2SO_4 , 0.0625 M $\text{H}_2\text{SO}_4/0.0625\%$ NaCl and 0.0625 M $\text{H}_2\text{SO}_4/2\%$ NaCl solutions.

The optical images in Figure 3b depict general surface deterioration due to the reaction effect of SO_4^{2-} anions within the electrolyte compared with Figure 3a. In the presence of a low Cl^- anion concentration, the competitive adsorption/reaction of Cl^- and SO_4^{2-} anion results in a superficial general surface deterioration at a magnification of $\times 10$ and visible localized deterioration of Zn surface at a magnification of $\times 100$. At a 2% Cl^- anion concentration, the extent of Zn surface deterioration is very severe (Figure 3d). Table 1 shows a progressive increase in the Zn corrosion rate values. The corrosion reactions occur at the metal–solution interface within the acid chloride solution [32]. The corrosion rates vary from 4.089 mm/year in a 0.0625 M H_2SO_4 solution to 10.085 mm/year in a 0.0625 M $\text{H}_2\text{SO}_4/2\%$ NaCl concentration. At 0.0625 M H_2SO_4 to 0.0625 M $\text{H}_2\text{SO}_4/0.125\%$ NaCl concentrations, the variation in the corrosion rate is minimal due to the effective protection of the Zn surface within the electrolyte by ZnO. However, at a 0.0625 M $\text{H}_2\text{SO}_4/0.25\%$ NaCl concentration, the corrosion rate of Zn

significantly increases to 5.259 mm/year, indicating the threshold Cl^- anion concentration for accelerated corrosion. This observation continued till a 0.0625 M $\text{H}_2\text{SO}_4/2\%$ NaCl concentration. The polarization plots from 0.0625 M $\text{H}_2\text{SO}_4/0.25\%$ NaCl to 0.0625 M $\text{H}_2\text{SO}_4/2\%$ NaCl show a cathodic potential shift in agreement with an increase in the Zn corrosion rate analogous to the Cl^- anion concentration. This occurred with an increase in the anodic/cathodic Tafel plots.

3.2 Open-circuit potential and XRF analysis

The open-circuit potential plots for Zn corrosion in 0.0625 M H_2SO_4 , 0.0625 M $\text{H}_2\text{SO}_4/0.0625\%$ NaCl and 0.0625 M $\text{H}_2\text{SO}_4/2\%$ NaCl solutions are presented in Figure 4. Table 2 depicts the XRF results retrieved from the analysis of Zn surfaces prior to corrosion and following corrosion in the solutions mentioned earlier. The Zn plot in a 0.0625 M H_2SO_4 solution

Table 2: XRF analysis data on the concentration of oxides on Zn surfaces

| Oxides | As received | | 0.0625 M H_2SO_4 | | 0.0625 M $\text{H}_2\text{SO}_4/0.0625\%$ NaCl | | 0.0625 M $\text{H}_2\text{SO}_4/2\%$ NaCl | |
|-------------------------|-------------------|-------------------|----------------------------------|-------------------|--|-------------------|---|-------------------|
| | Counts per second | % Conc. of oxides | Counts per second | % Conc. of oxides | Counts per second | % Conc. of oxides | Counts per second | % Conc. of oxides |
| Fe_2O_3 | 8,378 | 3.03 | 6,315 | 0.292 | 1,526 | 0.268 | 6,201 | 0.292 |
| TiO_2 | 2,116 | 0.94 | 1,435 | 0.064 | 687 | 0.023 | 1,426 | 0.063 |
| CaO | 1,830 | 3.31 | 1,300 | 0.296 | 665 | 0.254 | 1,256 | 0.293 |
| K_2O | 791 | 0.5 | 590 | 0.025 | 297 | 0.148 | 595 | 0.024 |
| SiO_2 | 394 | 65.87 | 418 | 6.581 | 410 | 6.582 | 504 | 6.566 |
| ZnO | 175 | 0.6 | 204 | 92.8 | 180 | 90.4 | 336 | 91.2 |
| Al_2O_3 | 171 | 3.21 | 166 | 0.316 | 145 | 0.298 | 264 | 0.303 |
| MgO | 54 | 0.46 | 41 | 0.046 | 24 | 0.046 | 53 | 0.046 |

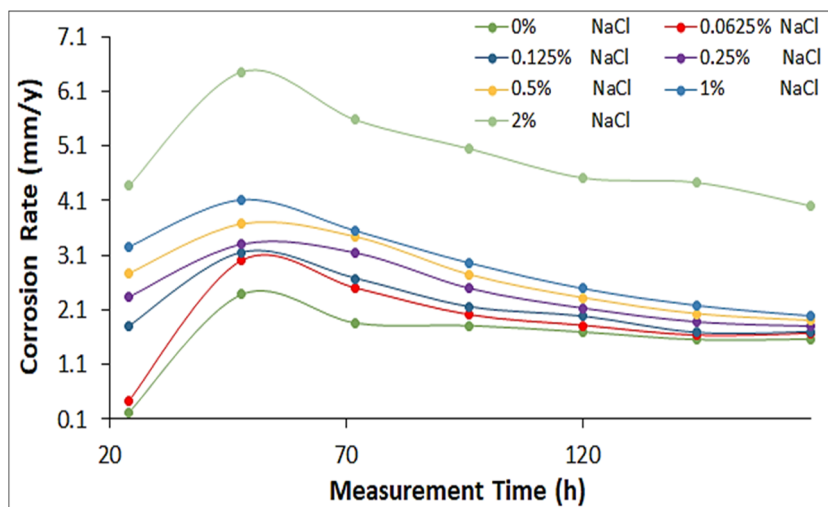


Figure 5: A corrosion rate plot for Zn corrosion in 0.00625 M H_2SO_4 to 0.0625 M $\text{H}_2\text{SO}_4/2\%$ NaCl solution.

exhibited the most electropositive data plots indicating higher resistance to surface oxidation. The plot initiated at -0.95 V (0 s) moderately increased to -0.92 V at 800.01 s of exposure due to the initial corrosion of the Zn surface before the onset of protective oxide formation. Beyond 800.01 s, the plot showed relative stability before culminating at -0.91 V (7,200 ns). Though the plot configuration indicates significant active/passive transition behavior on the Zn surface during exposure as the protective oxide on Zn continues to grow. The XRF data in Table 2 show that Fe_2O_3 , CaO , SiO_2 , Al_2O_3 and ZnO oxides exhibit the highest concentration among the oxides on the Zn surface before corrosion compared to the other oxides. The concentrations of these oxides (excluding ZnO) decreased in the acid and acid chloride electrolytes when compared to the values obtained for as-received Zn. Simultaneously, the concentration of ZnO significantly increased due to the redox reaction effect of the corrosive anions in H_2SO_4 and $\text{H}_2\text{SO}_4/\text{NaCl}$ solutions. In the presence of these corrosive species, ZnO is formed on the Zn surface. These oxides influenced the semi-conductor properties of Zn surfaces before and during the corrosion reaction processes, and hence, invariably the corrosion resistance of Zn and its thermodynamic properties. The Zn plot at 0.0625 M $\text{H}_2\text{SO}_4/2\%$ NaCl solution depicts the most electro-negative plot configuration due to the combined reaction effect of Cl^- and SO_4^{2-} anions in the electrolyte. The plot initiated at -1 V sharply increases to -0.97 V at 494.4 s. Beyond this point on the plot, the relative thermodynamic stability of the Zn surface was attained compared to the Zn plot at 0.00625 M H_2SO_4 . The plot eventually culminated at -0.96 V at 7,200 s of exposure. The corrosion potential values of the plots align with the results obtained from potentiodynamic polarization where an increase in the Cl^- anion

concentration leads to the breakdown of the protective oxide on the Zn surface and exposure of the substrate metal to corrosion.

3.3 SEM, EDX and weight loss analysis

The weight loss data of Zn corrosion at a specific Cl^- anion concentration are presented in Figure 5. Table 3 indicates the weight loss data at 168 h of examination. SEM images (mag. $\times 2,000$ and $\times 3,000$) of Zn before corrosion, after corrosion in a 0.0625 M H_2SO_4 solution and after corrosion in a 0.00625 M $\text{H}_2\text{SO}_4/2\%$ NaCl solution are shown in Figure 6a–c. Table 4 shows the EDX data for the SEM images. The weight loss data plots show that the Zn corrosion behavior at a specific Cl^- anion concentration depicts a similar plot configuration throughout the exposure hours signifying similar redox reaction processes of Zn in the acid electrolyte. However, the corrosion rates increased with an increase in the Cl^- anion concentration. It is also observed

Table 3: Weight loss data for Zn corrosion in a 0.0625 M H_2SO_4 solution at 0.0625–2% NaCl concentration at 168 h of exposure

| NaCl concentration (%) | Weight loss, W_L (g) | Corrosion rate, C_{RT} (mm/year) |
|------------------------|------------------------|------------------------------------|
| 0 | 0.196 | 1.562 |
| 0.0625 | 0.209 | 1.670 |
| 0.125 | 0.213 | 1.700 |
| 0.25 | 0.225 | 1.798 |
| 0.5 | 0.239 | 1.906 |
| 1 | 0.249 | 1.990 |
| 2 | 0.503 | 4.015 |

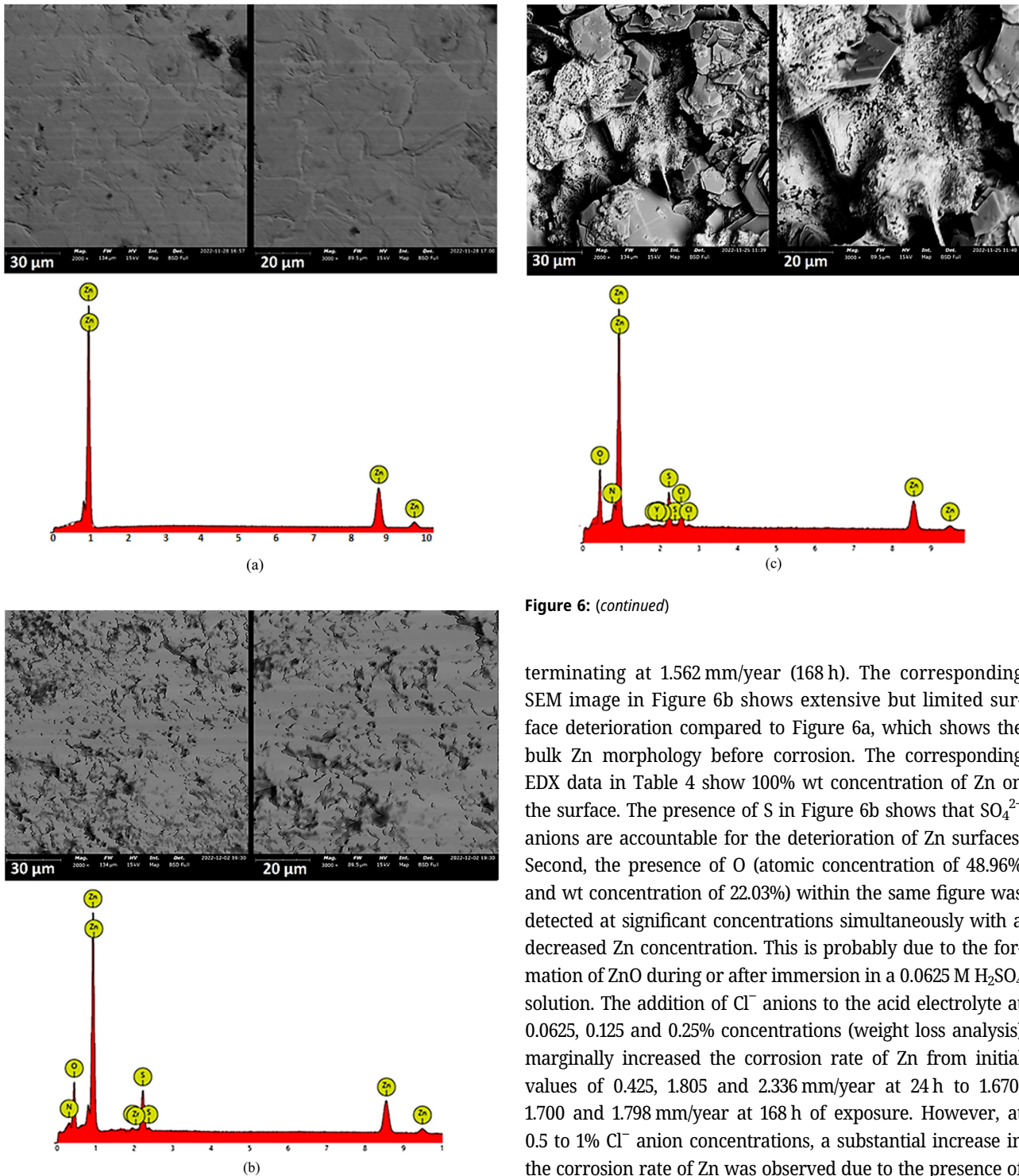


Figure 6: (continued)

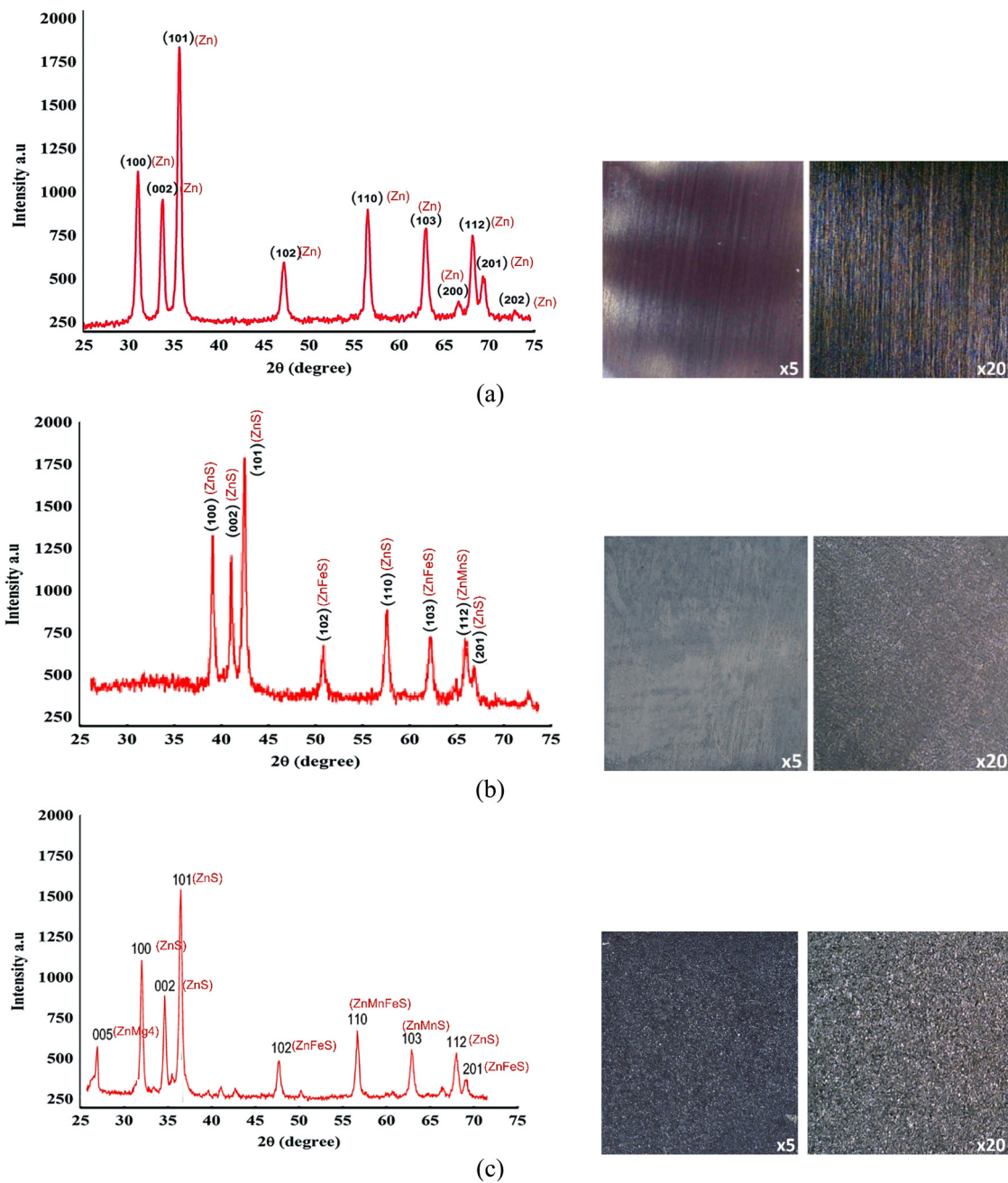
terminating at 1.562 mm/year (168 h). The corresponding SEM image in Figure 6b shows extensive but limited surface deterioration compared to Figure 6a, which shows the bulk Zn morphology before corrosion. The corresponding EDX data in Table 4 show 100% wt concentration of Zn on the surface. The presence of S in Figure 6b shows that SO_4^{2-} anions are accountable for the deterioration of Zn surfaces. Second, the presence of O (atomic concentration of 48.96% and wt concentration of 22.03%) within the same figure was detected at significant concentrations simultaneously with a decreased Zn concentration. This is probably due to the formation of ZnO during or after immersion in a 0.0625 M H_2SO_4 solution. The addition of Cl^- anions to the acid electrolyte at 0.0625, 0.125 and 0.25% concentrations (weight loss analysis) marginally increased the corrosion rate of Zn from initial values of 0.425, 1.805 and 2.336 mm/year at 24 h to 1.670, 1.700 and 1.798 mm/year at 168 h of exposure. However, at 0.5 to 1% Cl^- anion concentrations, a substantial increase in the corrosion rate of Zn was observed due to the presence of excess Cl^- anions in the acid electrolyte. At a 2% Cl^- anion concentration, the corrosion rate of Zn significantly increased between 4.376 mm/y at 24 h and 4.015 mm/year at 168 h. Figure 6c shows a visible degraded Zn morphology due to the electrochemical action of SO_4^{2-} and Cl^- anions. The corresponding EDX data (Table 4) show a significant presence of S, Cl and O, which are actively involved in the redox electrochemical reactions taking place on Zn surfaces.

Figure 6: SEM images and EDX data for Zn: (a) preceding corrosion test, (b) following corrosion in 0.0625 M H_2SO_4 solution and (c) following corrosion in a 0.0625 M H_2SO_4 /2% NaCl solution.

that the corrosion rate of Zn at all concentrations generally decreased after 48 h of exposure to 168 h. At 0% Cl^- anion concentration, the corrosion rate initiated at 0.218 mm/year progressively increased to 2.381 mm/year (48 h) before

Table 4: EDX data for Zn preceding the corrosion test, following corrosion in 0.0625 M H₂SO₄ solution and following corrosion in a 0.0625 M H₂SO₄/2% NaCl solution

| Zn | | | Zn in 0.0625 M H ₂ SO ₄ | | | Zn in 0.0625 M H ₂ SO ₄ /2% NaCl | | |
|----------------|--------------|--------------|---|--------------|--------------|--|--------------|--------------|
| Element symbol | Atomic conc. | Weight conc. | Element symbol | Atomic conc. | Weight conc. | Element symbol | Atomic conc. | Weight conc. |
| Zn | 100 | 100 | O | 51.66 | 22.93 | Zn | 90.19 | 97.02 |
| | | | Zn | 38.24 | 66.98 | O | 8.47 | 2.23 |
| | | | S | 8.81 | 7.94 | Cl | 0.68 | 0.40 |
| | | | N | 0.60 | 1.21 | S | 0.66 | 0.35 |
| | | | Zr | 0.48 | 0.95 | | | |

**Figure 7:** XRD peaks for Zn: (a) preceding corrosion, (b) following corrosion in a 0.0625 M H₂SO₄ solution and (c) following corrosion in a 0.0625 M H₂SO₄/2% NaCl solution.

3.4 XRD

XRD of Zn after application of electrochemical techniques in the acid chloride electrolyte prior to corrosion, following corrosion in 0.0625 M H₂SO₄, and following corrosion in 0.0625 M H₂SO₄/2% NaCl solution was performed, and the results are shown in Figure 7–c. The figures also depict the corresponding optical images of the Zn surface at magnifications of ×5 and ×20. The diffraction peaks shown in Figure 7a (Zn(002), Zn(100), Zn(101), Zn(102), Zn(103), Zn(110), Zn(112), Zn(200) and Zn(201)) generally indicate the presence of a pure Zn metal and its crystalline nature [33,34]. The corresponding peaks occurred at $2\theta = 30.3^\circ$, 34.5° , 35.8° , 46.5° , 55.5° , 63.2° , 66.3° , 68.6° , 70.2° and 73.3° for Zn before the corrosion test. The highest peaks in these figures occurred at 30.3° , 34.5° and 35.8° , which match the Zn (100), Zn (101) and Zn (002) phases, respectively [35]. Most corrosion products on Zn surfaces are crystalline, and insoluble and tend to add to the corrosion resistance of the Zn H₂SO₄ solution [36]. The peak data in Figure 7b at $2\theta = 38.5^\circ$, 40.4° , 42.6° , 50.4° , 57.1° , 64.5° , 65.6° , 66.3° and 73.5° generally indicate the presence of ZnS, ZnFeS and ZnMnS. The peak data of Figure 7c ($2\theta = 26.5^\circ$, 30.4° , 35.6° , 36.4° , 40.1° , 42.3° , 47.4° , 50.2° , 55.3° , 63.4° , 66.4° , 67.2° and 67.3°) show the presence of ZnS, ZnFeS and ZnMnS, ZnMg₄ and ZnMnFeS phases compared to the presence of impurities detected with EDX and XRF analysis.

4 Conclusion

Zn exhibited intermediate resistance to corrosion in a 0.0625 M H₂SO₄ solution and within it at low Cl⁻ anion concentrations where the reactive/inert transition behavior of the corrosion polarization plots was marginal. A higher Cl⁻ anion concentration above 0.5% results in a significant anodic corrosion potential shift and extensive localized and general morphological deterioration of the metal. Variation in the Cl⁻ anion concentration has limited influence on the corrosion properties of Zn analogous to exposure times, despite an increase in the corrosion rate. EDX analysis before corrosion indicates 100% Zn content, wt%. Although, the exposure to H₂SO₄ captures the presence of S while Cl was captured in the presence of Cl⁻ anions. However, the presence of other impurity elements in trace concentrations was discovered after the partial destruction of the Zn substrate metal. The open-circuit potential plots of Zn in the acid chloride solution indicate limited thermodynamic instability on Zn surfaces. However, the Cl⁻ anion concentration dictates the potential shifts of

the plots. Crystallographic phases and compounds on Zn were significantly influenced by the electrochemical action of Cl⁻ and SO₄²⁻ anions.

Acknowledgement: The author appreciates the financial contribution and support of Covenant University toward the success of the research.

Conflict of interest: The author states no conflict of interest.

References

- [1] Serosh E, Bernd H, Volker S. A review of the development and application of microalloyed medium carbon steels. *Steel Res.* 1987;58(8):369–76.
- [2] Han D, Xinjun S. Deformation induced ferrite transformation in low carbon steels. *Curr Opin Solid State Mater Sci.* 2005;9(6):269–76.
- [3] Deepak D, Kateřina L, Thomas B. Carbon steel corrosion: A review of key surface properties and characterization methods. *RSC Adv.* 2017;7:4580–610.
- [4] Siddiqui RA, Hussein AA. Hydrogen embrittlement in 0.31% carbon steel used for petrochemical applications. *J Mater Process Technol.* 2005;170(1–2):430–5.
- [5] Edmonds DV, Cochrane RC. The effect of alloying on the resistance of carbon steel for oilfield applications to CO₂ corrosion. *Mater Res.* 2005;8(4):377–85. doi: 10.1590/S1516-143920050004000004.
- [6] Akpanyung KV, Loto RT, Fajobi MA. An overview of Ammonium Chloride (NH₄Cl) corrosion in the refining unit. *J Phys Conf Ser.* 2019;1378(2):022089. doi: 10.1088/1742-6596/1378/2/022089.
- [7] Faisal M, Gusai A, Erin VI, Keller MW, Shirazi S, Roberts KP. Mechanistic modeling of erosion–corrosion for carbon steel. *Trends Oil Gas Corros Res Technol.* 2017;749–63. doi: 10.1016/B978-0-08-101105-8.00031-0.
- [8] Cai J, Sun L, Ma H, Xiaogang L. Corrosion characteristics of Q690qE high-strength bridge steel in simulated coastal–industrial environment and its influence on mechanical and corrosion fatigue behaviors. *Constr Build Mater.* 2022;341:127830. doi: 10.1016/j.conbuildmat.2022.127830.
- [9] Zhang W, Yang S, Wen-Tong G, Qiang H, Lujun Z. Corrosion behavior of the low alloy weathering steels coupled with stainless steel in simulated open atmosphere. *Mater Chem Phys.* 2022;288:126409. doi: 10.1016/j.matchemphys.2022.126409.
- [10] Loto RT. Pitting corrosion evaluation and inhibition of stainless steels: A review. *J Mats Env Sci.* 2015;6(10):2750–62.
- [11] Loto RT. Anti-corrosion performance of the synergistic properties of benzenecarbonitrile and 5-bromovanillin on 1018 carbon steel in HCl environment. *Sci Rep.* 2017;7(1):17555.
- [12] Ping L, Min D. Effect of chloride ion content on pitting corrosion of dispersion-strengthened-high-strength steel. *Corros Commun.* 2022;7:23–34. doi: 10.1016/j.corcom.2022.03.005.
- [13] Kuklík V, Kudláček J. List of selected zinc coating technologies. Hot-dip galvanizing of steel structures. Amsterdam: Elsevier; 2016. p. 1–5. doi: 10.1016/C2014-0-03512-5.
- [14] Zhang XG. Corrosion of zinc and zinc alloys. In *ASM HandBook, corrosion: Materials.* Ohio: ASM International; vol. 13B, 2005. doi: 10.31399/asm.hb.v13b.a0003830.

- [15] Zinc Statistics and Information, National minerals information center. <https://www.usgs.gov/centers/national-minerals-information-center/zinc-statistics-and-information>. Retrieved November 3, 2022.
- [16] Greenwood NN, Earnshaw A. Chemistry of the elements. 2nd edn. Oxford: Butterworth-Heinemann; 1997.
- [17] Emsley J. "Zinc". Nature's building blocks: An A-Z guide to the elements. Oxford, England: Oxford University Press; 2001. p. 499–50.
- [18] Zhang ZJ. Corrosion and electrochemistry of zinc. New York: Springer; 1996. p. 93.
- [19] American conference of governmental industrial hygienists - Documentation of the TLVs and BEIs. 7th edn. Cincinnati: ACGIH Worldwide; 2020.
- [20] Veleva L, Meraz E, Acosta M. Zinc precipitation runoff from galvanized steel in humid tropical climate. *Corros Eng Sci Technol*. 2010;45(1):76–83. doi: 10.1179/174327809X457030.
- [21] Veleva L, Kane RD. Atmospheric corrosion. In: Covino BS, Jr., Cramer SD, (editors.). *ASTM Handbook*, Vol. 13A, Ohio: ASM International Materials Park; 2003. p. 196–209.
- [22] Porter FC. Corrosion resistance of zinc and zinc alloys. Boca Raton: CRC Press; 1994. p. 121.
- [23] Deepti J, Shubhra P, Arunava A, Shrivastava R, Sassi W, Saroj KP, et al. Effect of exposure time on corrosion behavior of zinc-alloy in simulated body fluid solution: Electrochemical and surface investigation. *J Mater Res Technol*. 2021;10:738–51. doi: 10.1016/j.jmrt.2020.12.050.
- [24] Wallinder O, Leygraf C. A critical review on corrosion and runoff from zinc and zinc-based alloys in atmospheric environments. *Corrosion*. 2017;73(9):1060–77. doi: 10.5006/2458.
- [25] Rakel L, Jan-Erik S, Lars-Gunnar J. The atmospheric corrosion of zinc in the presence of NaCl. The influence of carbon dioxide and temperature. *J Electrochem Soc*. 2000;147(5). doi: 10.1149/1.1393429.
- [26] Zhang X. Corrosion and electrochemistry of Zinc. New York: Springer Science + Business Media. 1996. p. 481.
- [27] Neufeld A, Cole I, Bond A, Furman S. The initiation mechanism of corrosion of zinc by sodium chloride particle deposition. *Corros Sci*. 2002;3:555–72.
- [28] Farrow LA, Graedel TE, Leygraf C. GILDES model studies of aqueous chemistry. II. The corrosion of zinc in gaseous exposure chambers. *Corros Sci*. 1996;38(12):2181–99.
- [29] Mouanga M, Ricq L, Douglade G, Douglade J, Berçot P. Influence of coumarin on zinc electrodeposition. *Surf Coat Technol*. 2006;201:762–7.
- [30] Qing Q, Chuanwei Y, Ye, Wan Y, Cao C. Effects of NaCl and SO₂ on the initial atmospheric corrosion of zinc. *Corros Sci*. 2002;44(12):2789–803.
- [31] Roh B, Macdonald DD. The passivity of titanium—part III: characterization of the anodic oxide film. *J Solid State Electrochem*. 2019;23:2001–8. doi: 10.1007/s10008-019-04255-z.
- [32] Zhang L, Duan Y, Gao R, Yang J, Wei K, Tang D, et al. The effect of potential on surface characteristic and corrosion resistance of anodic oxide film formed on commercial pure titanium at the potentiodynamic-aging mode. *Materials (Basel)*. 2019;12(3):370. doi: 10.3390/ma12030370.
- [33] Leygraf C. Atmospheric corrosion. *Encyclopedia of Electrochemistry*. New York: Plenum Press; 2007.
- [34] Yuanyuan C, Shixiang L, Wenguo X, Huidong W, Juan W. Fabrication of superhydrophobic Au–Zn alloy surface on a zinc substrate for roll-down, selfcleaning and anti-corrosion properties. *J Mater Chem A*. 2015;3:16774.
- [35] Shams A, Zhanga Y, Khan F. Electrochemical behaviour and analysis of Zn and Zn–Ni alloy anti-corrosive coatings deposited from citrate baths. *RSC Adv*. 2018;8:28861–73.
- [36] Zhang XG. Corrosion and electrochemistry of zinc. New York: Plenum Press; 1996.